

1 **Measurement Report: Effects of anthropogenic emissions and**  
2 **environmental factors on biogenic secondary organic aerosol**  
3 **(BSOA) formation in a coastal city of Southeastern China**

4

5 Youwei Hong<sup>a,b,c,d\*</sup>, Xinbei Xu<sup>a,b,c</sup>, Dan Liao<sup>e</sup>, Taotao Liu<sup>a,b,c</sup>, Xiaoting Ji<sup>a,b,c</sup>, Ke Xu<sup>a,b,d</sup>,  
6 Chunyang Liao<sup>f</sup>, Ting Wang<sup>g</sup>, Chunshui Lin<sup>g</sup>, Jinsheng Chen<sup>a,b,c\*</sup>

7

8 <sup>a</sup>Center for Excellence in Regional Atmospheric Environment, Institute of Urban Environment,  
9 Chinese Academy of Sciences, Xiamen, 361021, China

10 <sup>b</sup>Key Lab of Urban Environment and Health, Institute of Urban Environment, Chinese Academy  
11 of Sciences, Xiamen, 361021, China

12 <sup>c</sup>University of Chinese Academy of Sciences, Beijing, 100049, China

13 <sup>d</sup>School of Life Sciences, Hebei University, Baoding, 071000, China

14 <sup>e</sup>College of Environment and Public Health, Xiamen Huaxia University, Xiamen 361024, China

15 <sup>f</sup>State Key Laboratory of Environmental Chemistry and Ecotoxicology, Research Center for Eco-  
16 Environmental Sciences, Chinese Academy of Sciences, Beijing 100085, China

17 <sup>g</sup> Institute of Earth Environment, Chinese Academy of Sciences, Xi'an, 710061, China

18

19 \*Corresponding author E-mail: Jinsheng Chen ([jschen@iue.ac.cn](mailto:jschen@iue.ac.cn)); Youwei Hong  
20 ([ywhong@iue.ac.cn](mailto:ywhong@iue.ac.cn))

21

22

23

24

25

26

27

28

29

30

31

32

33

34 **Abstract:**

35 To better understand the formation of biogenic secondary organic aerosol (BSOA),  
36 aerosol samples with a 4 h time resolution were collected during summer and  
37 wintertime in the southeast of China, along with on-line measurements of trace gases,  
38 aerosol chemical compositions, and meteorological parameters. The samples were  
39 analyzed by gas chromatography-mass spectrometry for PM<sub>2.5</sub>-bound SOA tracers,  
40 including isoprene (SOA<sub>I</sub>),  $\alpha/\beta$ -pinene (SOA<sub>M</sub>),  $\beta$ -caryophyllene (SOA<sub>C</sub>), and toluene  
41 (ASOA). The average concentrations of total SOA tracers in winter and summer were  
42 38.8 and 111.9 ng m<sup>-3</sup>, respectively, with the predominance of SOA<sub>M</sub> (70.1% and  
43 45.8%), followed by SOA<sub>I</sub> (14.0% and 45.6%), ASOA (11.0% and 6.2%) and SOA<sub>C</sub>  
44 (4.9% and 2.3%). Compare to those in winter, the majority of BSOA tracers in summer  
45 showed significant positive correlations with Ox (O<sub>3</sub>+NO<sub>2</sub>), HONO, ultraviolet (UV)  
46 and temperature (T), indicating the influence of photochemical oxidation under  
47 relatively clean conditions. However, in winter, BSOA tracers were significantly  
48 correlated with PM<sub>2.5</sub>, NO<sub>3</sub><sup>-</sup>, SO<sub>4</sub><sup>2-</sup>, and NH<sub>3</sub>, attributed to the contributions of  
49 anthropogenic emissions. Major BSOA tracers in both seasons was linearly correlated  
50 with aerosol acidity (pH), liquid water content (LWC) and SO<sub>4</sub><sup>2-</sup>. The results indicated  
51 that acid-catalyzed reactive uptake onto sulfate aerosol particles enhanced the  
52 formation of BSOA. In summer, the clean air mass originated from the ocean, and  
53 chlorine depletion was observed. We also found that concentrations of the total SOA  
54 tracers was correlated with HCl and chlorine ions in PM<sub>2.5</sub>, reflecting the contribution  
55 of Cl-initiated VOC oxidations to the formation of SOA. In winter, the northeast  
56 dominant wind direction brought continental polluted air mass to the monitoring site,  
57 affecting the transformation of BSOA tracers. This implied that anthropogenic  
58 emissions, atmospheric oxidation capacity and halogen chemistry have significant  
59 effects on the formation of BSOA in the southeast coastal area.

60 **Keywords:** SOA tracers; biogenic volatile organic compounds; anthropogenic  
61 pollutants; atmospheric oxidation capacity; coastal area

62

## 63 **1. Introduction**

64 Secondary organic aerosol (SOA) has attracted widespread scientific researchers  
65 concerns, due to its potential impacts on climate change, human health and air quality  
66 (Shrivastava et al., 2017; Reid et al., 2018; Zhu et al., 2019; Wang et al., 2021b).  
67 Understanding the formation of SOA and assessing its relevance for environmental  
68 effects become an integral part of aerosol chemistry (Charan et al., 2019; Xiao et al.,  
69 2020; Palmer et al., 2022). However, due to its complex precursors and atmospheric  
70 physical or chemical processes, SOA prediction by air quality models remains highly  
71 uncertain (McFiggans et al., 2019). Therefore, it is necessary to better explore missed  
72 SOA sources and unknown SOA formation mechanisms.

73 SOA was produced by the conversion of biogenic and anthropogenic volatile  
74 organic compounds (BVOCs and AVOCs) through complex homogeneous and  
75 heterogeneous reactions (Charan et al., 2019; Xiao et al., 2020; Mahilang et al., 2021).  
76 BVOCs are the main precursors of SOA on a global scale, while AVOCs are the  
77 predominant contributor to SOA in urban areas (Hallquist et al., 2009; Wang et al.,  
78 2021a). Recently, laboratory, field observation and model studies have shown that  
79 anthropogenic emissions greatly affect the formation of BSOA (Hoyle et al., 2011;  
80 Shrivastava et al., 2019; Zhang et al., 2019b; Zhang et al., 2019c; Mahilang et al., 2021;  
81 Xu et al., 2021). Anthropogenic air pollutants, such as NO<sub>x</sub>, SO<sub>2</sub>, NH<sub>3</sub> and aerosols,  
82 could influence the conversion of BVOCs to the particulate phase and the production  
83 of nitrogen and sulfur compounds (Wang et al., 2020). NO<sub>x</sub> is one of the important  
84 drivers of SOA formation and yields during both daytime and nighttime through  
85 alternating the fate of peroxy radicals (RO<sub>2</sub>·) (Sarrafzadeh et al., 2016; Newland et al.,  
86 2021). While ·OH dominates the photochemical oxidation of BVOC during daylight  
87 hours, and NO<sub>3</sub>· becomes one of the main oxidants for biogenic SOA and organic  
88 nitrates at night. SO<sub>2</sub> also plays an important role in changing SOA formation from  
89 BVOC photooxidation and ozonolysis through sulfuric acid formation and acid-  
90 catalyzed heterogeneous reactions (Zhao et al., 2018; Zhang et al., 2019b; Xu et al.,

91 2021). In addition, NH<sub>3</sub> and amines can affect the SOA yields and composition through  
92 both gas-phase and heterogeneous reactions, by reacting with sulfuric or nitric acid to  
93 generate secondary inorganic aerosols (SIA) (Ma et al., 2018; Liu et al., 2021; Lv et  
94 al.,2022). However, due to complex precursors and atmospheric processes, the  
95 combined effects of anthropogenic emissions and meteorological factors on the  
96 formation of SOA are not fully understood.

97 The coastal area of southeastern China is under the East Asian monsoon control,  
98 which cause an obvious alternation of polluted and clean air masses from continental  
99 and ocean area, respectively (Wu et al., 2019; Hong et al., 2021). Also, the local  
100 geographical environment, including relatively high humidity, dense vegetation and  
101 strong atmospheric oxidation capacity, provides a good chance to study the sources and  
102 formation mechanisms of SOA. In our previous studies, ground-based observations in  
103 a mountainous forest area of this region showed that BSOA tracers were the largest  
104 contributor to SOA, and the aerosols were highly oxidized (Hong et al., 2019). However,  
105 with the development of rapid urbanization, anthropogenic emissions will be of great  
106 significance on SOA formation (Liu et al., 2020). Halogen radicals (chlorine, bromine,  
107 iodine) have an important role in tropospheric oxidants chemistry and OA formation  
108 (Wang et al., 2021c). Therefore, it is necessary to investigate the sources and formation  
109 mechanisms of SOA in coastal urban areas, and so as to provide a scientific basis for  
110 the estimation of regional SOA budgets and PM<sub>2.5</sub> pollution control.

111 In this study, a continuous PM<sub>2.5</sub> sampling campaign with a 4 h time resolution  
112 was conducted in a coastal city of southeastern China during the winter and  
113 summertime period. Seasonal, diurnal variations and SOC contributions of SOA tracers  
114 were analyzed. We also demonstrated the indications of SOA tracers for air pollution  
115 process. Finally, the combined effects of anthropogenic emissions and major  
116 environmental factors on promoting SOA formation was discussed.

## 117 **2. Materials and methods**

### 118 *2.1 Sample collection*

119 The sampling was performed at the Institute of Urban Environment, Chinese  
120 Academy of Sciences (118.06° E, 24.61° N), which is located in a suburban area of  
121 Xiamen, a coastal city of southeastern China. Detailed information of the air monitoring  
122 supersite was described in our previous study (Hong et al., 2021). Briefly, time-resolved  
123 (00:00–08:00, 08:00–12:00, 12:00–16:00, 16:00–20:00, 20:00–24:00 CST – China  
124 Standard Time) PM<sub>2.5</sub> samples were collected on the rooftop of the station (about 70m  
125 above the ground). The sampling was carried out by using a high volume (1.05 m<sup>3</sup> min<sup>-1</sup>)  
126 sampler (TH-1000C, Wuhan Tianhong, China) with a PM<sub>2.5</sub> inlet from 10 to 18 January,  
127 and from 5 to 14 July 2020. All samples were collected onto pre-baked (450 °C, 6 h)  
128 quartz fiber filters. Field blank samples were also collected. The sample filters were  
129 separately sealed in aluminum foil and stored in a freezer (–20 °C) prior to analysis.

### 130 2.2 SOA tracers analysis by GC/MS

131 The isoprene-derived SOA (SOA<sub>I</sub>) tracers included 2 methyltetrols (MTLs: 2-  
132 methylthreitol (MTL1) and 2-methylerythritol (MTL2)), C5-alkene triols (cis-2-  
133 methyl-1,3,4-trihydroxy-1-butene, trans-2-methyl-1,3,4-trihydroxy-1-butene, and 3-  
134 methyl-2,3,4-trihydroxy-1-butene) and 2-methylglyceric acid (MGA). The  
135 monoterpene-derived SOA (SOA<sub>M</sub>) tracers were composed of pinic acid (PA), pinonic  
136 acid (PNA), 3-hydroxyglutaric acid (HGA), 3-methyl-1,2,3-butanetricarboxylic acid  
137 (MBTCA), 3-hydro-4,4-dimethylglutaric acid (HDMGA), and 3-acetylglutaric acid  
138 (AGA). The β-caryophyllene-derived SOA (SOA<sub>C</sub>) tracer was β-caryophyllenic acid  
139 (CA), the toluene-derived SOA (SOA<sub>A</sub>) tracer was 2,3-Dihydroxy-4-oxopentanoic acid  
140 (DHOPA) and levoglucosan (LEV) as a tracer of biomass burning. Due to the lack of  
141 authentic standards, surrogate standards (including erythritol, malic acid, PA and  
142 citramalic acid) were used to compensate for unavoidable assay variance of SOA<sub>I</sub>,  
143 SOA<sub>M</sub>, SOA<sub>C</sub> and SOA<sub>A</sub> tracer in each sample during the pretreatment process,  
144 respectively (Fu et al., 2009).

145 The analytical procedure of fifteen SOA tracers was published in our previous  
146 studies (Hong et al., 2019; Liu et al., 2020). Briefly, the filter samples were  
147 ultrasonically extracted with a mixture of dichloromethane and methanol (2:1, v/v) for

148 10 min three times. The mixed extracts were filtered with a PTFE filter (0.22  $\mu\text{m}$ ), and  
149 dried with high purity  $\text{N}_2$  (99.99%), and then derivatized with 60  $\mu\text{L}$  of  
150 N,O-bis-(trimethylsilyl) trifluoroacetamide (BSTFA) with 1% trimethylsilyl chloride  
151 and 10  $\mu\text{L}$  of pyridine at 70  $^\circ\text{C}$  for 3 h. At last, 140  $\mu\text{L}$  of internal standard solution ( $^{13}\text{C}$   
152 n-alkane solution, 1.507  $\text{ng } \mu\text{L}^{-1}$ ) was added into the samples. Then, relative response  
153 factors (RRFs) of surrogate and internal standard were calculated to quantify the  
154 targeted organic tracers in each sample. Details of SOA tracer's calculated  
155 concentrations based on RRFs were presented in our previous studies (Hong et al., 2019;  
156 Liu et al., 2020).

157 Fifteen SOA tracers were determined by GC-MSD (7890A/5975C, Agilent  
158 Technologies, Inc., USA) with a DB-5 MS silica capillary column (i.d. 30 $\times$ 0.25 mm,  
159 0.25  $\mu\text{m}$  film thickness). 1  $\mu\text{L}$  sample was injected with splitless mode and high purity  
160 helium (99.999%) was used as carrier gas at a stable flow of 1.0 mL/min. The GC  
161 temperature was initiated at 100  $^\circ\text{C}$  (held for 1 min) and then to 300  $^\circ\text{C}$  at 5  $^\circ\text{C min}^{-1}$ ,  
162 and kept at 300  $^\circ\text{C}$  for 10 min. The operation mode is electron ionization (EI) mode of  
163 70 eV. The method detection limits (MDLs) for erythritol and PNA were 0.01 and 0.02  
164  $\text{ng m}^{-3}$ , respectively. The recoveries of erythritol, PNA, malic acid, PA and citramalic  
165 acid were 67 $\pm$ 2%, 73 $\pm$ 1%, 75 $\pm$ 1%, 88 $\pm$ 7% and 82 $\pm$ 8%, respectively. SOA tracers were  
166 not detected in the field blank samples.

### 167 *2.3 Observations in the air monitoring supersite*

168 Water-soluble inorganic ions (WSII) in  $\text{PM}_{2.5}$  ( $\text{Cl}^-$ ,  $\text{SO}_4^{2-}$ ,  $\text{NO}_3^-$ ,  $\text{Na}^+$ ,  $\text{K}^+$ ,  $\text{NH}_4^+$ ,  
169  $\text{Mg}^{2+}$ , and  $\text{Ca}^{2+}$ ) and gas pollutants (HCl, HONO,  $\text{HNO}_3$ ,  $\text{NH}_3$ ) were hourly measured  
170 using a monitoring device for aerosols and gases in ambient Air (MARGA 2080;  
171 Metrohm Applikon B.V.; Delft, Netherlands). Internal calibration was carried out using  
172 LiBr standard solutions. The detection limit of  $\text{Cl}^-$ ,  $\text{SO}_4^{2-}$ ,  $\text{NO}_3^-$ ,  $\text{Na}^+$ ,  $\text{K}^+$ ,  $\text{NH}_4^+$ ,  $\text{Mg}^{2+}$ ,  
173 and  $\text{Ca}^{2+}$  were 0.01, 0.04, 0.05, 0.05, 0.09, 0.05, 0.06 and 0.09  $\mu\text{g m}^{-3}$ , respectively.

174 Hourly mass concentrations of  $\text{PM}_{2.5}$  and  $\text{PM}_{10}$  were measured by using a tapered  
175 element oscillating microbalance (TEOM1405, Thermo Scientific Corp., MA, USA).  
176  $\text{NO}_2$ ,  $\text{SO}_2$ , and  $\text{O}_3$  were monitored using continuous gas analyzers (TEI 42i, 43i, and

177 49i, Thermo Scientific Corp., MA, USA). Ambient meteorological parameters  
178 including relative humidity (RH), temperature (T), wind speed (WS), and wind  
179 direction (WD) were obtained by an ultrasonic anemometer (150WX, Airmar, the  
180 USA). Photolysis frequencies were determined using a photolysis spectrometer (PFS-  
181 100, Focused Photonics Inc., Hangzhou, China), including the photolysis rate constants  
182  $J(\text{O}^1\text{D})$ ,  $J(\text{HCHO}_M)$ ,  $J(\text{HCHO}_R)$ ,  $J(\text{NO}_2)$ ,  $J(\text{H}_2\text{O}_2)$ ,  $J(\text{HONO})$ ,  $J(\text{NO}_3_M)$  and  
183  $J(\text{NO}_3_R)$ , and the spectral band ranged from 270 to 790 nm. Boundary layer height  
184 (BLH) based on ERA-5 reanalysis dataset was downloaded from the following link  
185 <https://www.ecmwf.int/en/forecasts/datasets/reanalysis-datasets/era5>.

#### 186 *2.4 Estimation of SOC using a tracer-based method*

187 The fraction of SOC formed by the oxidation of monoterpene, isoprene,  $\beta$ -  
188 caryophyllene and toluene was estimated using a tracer-based method (Kleindienst et  
189 al., 2007; Hong et al., 2019). It is defined as  $[\text{SOC}] = \sum i[\text{tri}]/f_{\text{SOC}}$ , where  $[\text{SOC}]$   
190 represents the mass concentration of SOC ( $\mu\text{gC m}^{-3}$ ) and  $\sum i[\text{tri}]$  means the sum of the  
191 concentration of individual SOA tracer ( $\mu\text{g m}^{-3}$ ). The carbon mass fractions ( $f_{\text{SOC}}$ ) of  
192 monoterpene, isoprene,  $\beta$ -caryophyllene and toluene were  $0.231 \pm 0.111$ ,  $0.155 \pm 0.039$ ,  
193  $0.023 \pm 0.005$  and  $0.008 \pm 0.003$ , respectively, based on smog-chamber experimental  
194 data (Kleindienst et al., 2007).

#### 195 *2.5 Aerosol acidity and OH calculation*

196 The forward mode of ISORROPIA II thermodynamic model was used to calculate  
197 the aerosol acidity (pH) (Fountoukis and Nenes, 2007). ISORROPIA II can calculate  
198 liquid water content (LWC), based on total  $\text{SO}_4^{2-}$ ,  $\text{NO}_3^-$ ,  $\text{Cl}^-$ , ammonia, non-volatile  
199 cations ( $\text{Na}^+$ ,  $\text{K}^+$ ,  $\text{Ca}^{2+}$ ,  $\text{Mg}^{2+}$ ), and meteorological factors (RH and T) (Rumsey et al.,  
200 2014; Guo et al., 2016). The pH value from ISORROPIA II was calculated using the  
201 following equation:

$$202 \quad \text{pH} = -\lg\left(\frac{1000 \times \text{H}^+}{\text{LWC}}\right)$$

203 where  $\text{H}^+$  is the hydronium ion concentration loading for an air sample ( $\mu\text{g}/\text{m}^3$ ).

204 The OH concentration ([OH]) was estimated using the NO<sub>2</sub> and HONO  
205 concentrations and the photolysis rate constants (J) of NO<sub>2</sub>, O<sub>3</sub>, and HONO, according  
206 to the following improved empirical formula (Wen et al., 2019).

$$207 \quad [\text{OH}] = 4.1 \times 10^9 \times \frac{J(\text{O}^1\text{D})^{0.83} \times J(\text{NO}_2)^{0.19} \times (140 \times \text{NO}_2 + 1) + \text{HONO} \times J(\text{HONO})}{0.41 \times \text{NO}_2^2 + 1.7 \times \text{NO}_2 + 1 + \text{NO} \times k_{\text{NO}+\text{OH}} + \text{HONO} \times k_{\text{HONO}+\text{OH}}}$$

## 208 2.6 Statistical analysis

209 Correlation analysis by SPSS 22.0 software (IBM, Armonk, NY, USA) was used  
210 to study the relationship among SOA tracers, meteorological parameters and criteria air  
211 pollutants. One-way analysis of variance (ANOVA) was adopted to examine the  
212 variations of different factors.

## 213 2.7. Backward trajectory analysis

214 Hybrid Single-Particle Lagrangian Integrated Trajectory (HYSPLIT) was used to  
215 analyze the impacts of air masses on Xiamen during different seasons. 72 h backward  
216 trajectories were calculated every hour at a height of 500 m. The meteorological data  
217 with a resolution of 1° longitude × 1° latitude was obtained from the NCEP/GDAS.  
218 Cluster analysis was adopted using the total spatial variance (TSV).

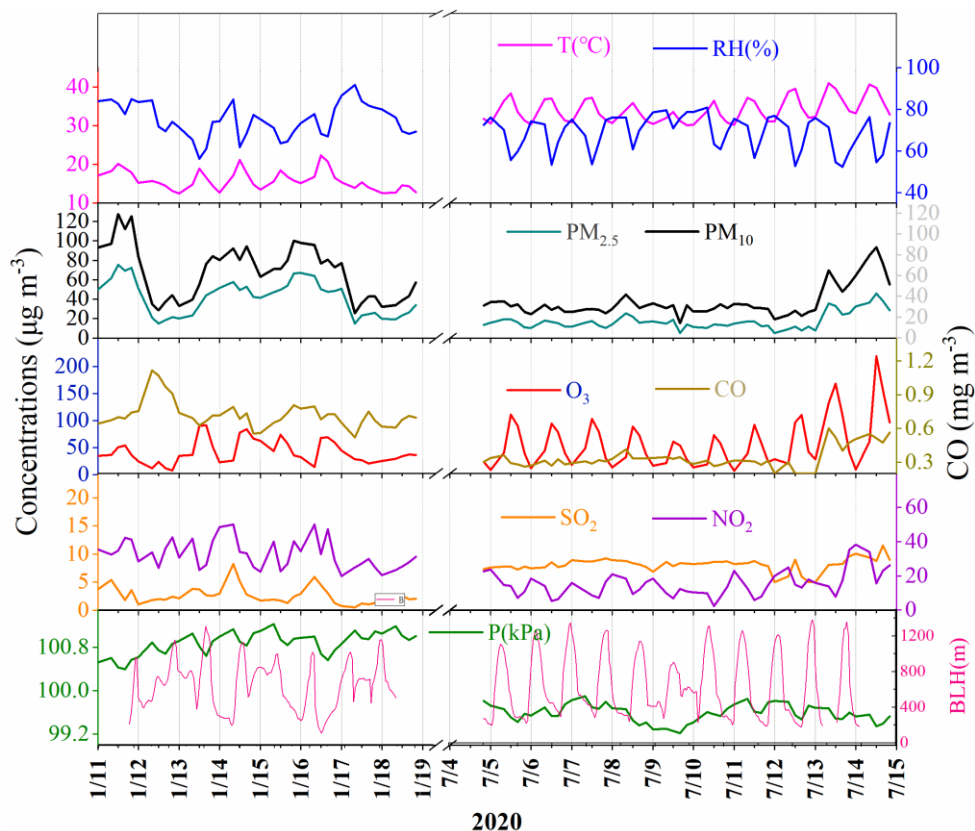
# 219 3 Results and discussion

## 220 3.1. Overview of air pollutants

221 The concentrations of criteria air pollutants, including SO<sub>2</sub>, CO, NO<sub>2</sub>, O<sub>3</sub>, PM<sub>2.5</sub>  
222 and PM<sub>10</sub>, and meteorological parameters during wintertime and summertime were  
223 shown in Fig.1. The concentrations of PM<sub>2.5</sub> in winter ranged from 14.9 to 75.3 μg m<sup>-3</sup>  
224 with an average of 42.1 μg m<sup>-3</sup>, which was much higher than that (the average of 18.4  
225 μg m<sup>-3</sup>) in summer, ranging from 12.8 to 46.4 μg m<sup>-3</sup>. The concentrations of CO, NO<sub>2</sub>  
226 and PM<sub>10</sub> showed similar seasonal trends to the pattern of PM<sub>2.5</sub>. In contrast, O<sub>3</sub> had the  
227 highest concentration in summer, which was attributed to the formation of  
228 photochemical reaction under strong UV radiation and the weak titration of nitrogen  
229 oxides. Meanwhile, the concentrations of SO<sub>2</sub> (8.37±0.79 μg m<sup>-3</sup>) in summer was also  
230 higher than that (2.63±1.95 μg m<sup>-3</sup>) in winter, mainly attributed to the influence of coal  
231 combustion and ship emissions. The monitoring site was located approximately 15 km



232 away from Xiamen port area and a coal-fired power plant ( $4 \times 300$  kW) in the south.  
 233 Southerly winds were prevailed in summer, which might cause the relative high  
 234 concentration of  $\text{SO}_2$  in the monitoring site.



235

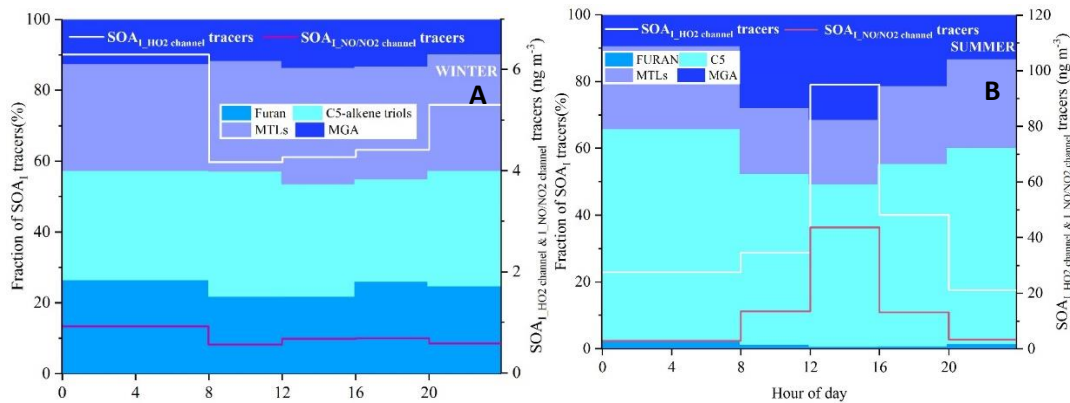
236 **Figure 1. Time series of criteria air pollutants and meteorological parameters**  
 237 **during the sampling period**

238 *3.2 Temporal variations of SOA tracers and estimated SOC*

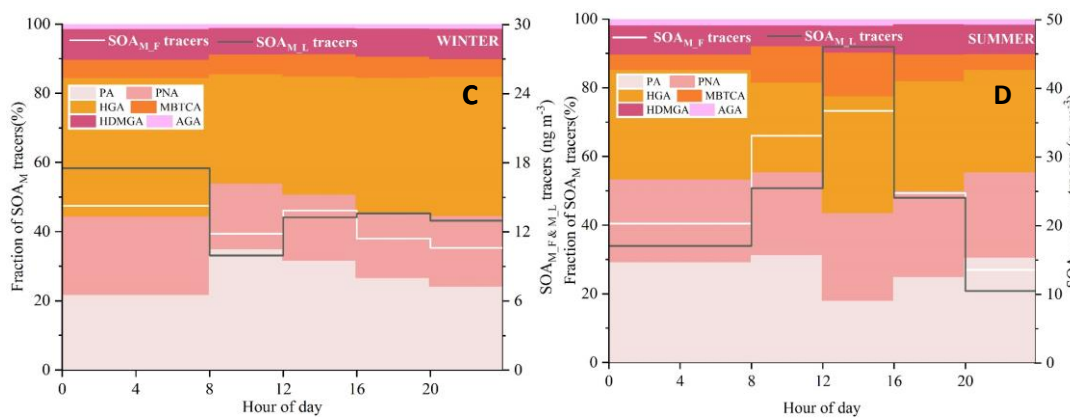
239 Temporal variations of individual SOA tracer are shown in Fig.S1. The average  
 240 concentrations of total SOA tracers in winter and summer were  $37.3$  and  $111.3 \text{ ng m}^{-3}$ ,  
 241 respectively. The predominance of  $\text{SOA}_M$  ( $26.6 \text{ ng m}^{-3}$ ), followed by  $\text{ASOA}$  ( $4.60 \text{ ng}$   
 242  $\text{m}^{-3}$ ),  $\text{SOA}_I$  ( $4.35 \text{ ng m}^{-3}$ ) and  $\text{SOA}_C$  ( $1.76 \text{ ng m}^{-3}$ ) was observed in winter while  $\text{SOA}_I$   
 243 ( $54.4 \text{ ng m}^{-3}$ ) and  $\text{SOA}_M$  ( $47.8 \text{ ng m}^{-3}$ ) in summer were the main contributors to total  
 244 SOA tracers, followed by  $\text{ASOA}$  ( $6.64 \text{ ng m}^{-3}$ ) and  $\text{SOA}_C$  ( $2.45 \text{ ng m}^{-3}$ ). In summer,  
 245 BSOA tracers showed much higher concentrations in the daytime ( $149.3 \text{ ng m}^{-3}$ ) than  
 246 in the nighttime ( $60.1 \text{ ng m}^{-3}$ ), while inverse results were observed in winter ( $30.4 \text{ ng}$   
 247  $\text{m}^{-3}$  and  $35.0 \text{ ng m}^{-3}$  in the daytime and nighttime, respectively). As shown in Table S2,

248 in summer, SOA<sub>I</sub> in the daytime ranged from 21.3 to 293.2 ng m<sup>-3</sup> (average of  
249 82.0±66.2 ng m<sup>-3</sup>) and the concentrations of SOA<sub>I</sub> ranging from 6.81 to 110.1 ng m<sup>-3</sup>  
250 (average of 26.8±24.6 ng m<sup>-3</sup>) were observed in the nighttime. However, in winter, the  
251 concentrations of isoprene SOA tracers in the daytime ranging from 1.36 to 11.1 ng m<sup>-3</sup>  
252 (average of 3.79±2.37ng m<sup>-3</sup>) were lower than those (average of 4.91±3.75 ng m<sup>-3</sup>) in  
253 the nighttime. As shown in Fig. 2, diurnal variations of SOA<sub>M</sub>, SOA<sub>I</sub>, CPA and DHOPA  
254 tracers in summer showed high levels in the afternoon (12:00–16:00 CST), due to the  
255 impacts of beneficial photochemical oxidation conditions caused by high temperature  
256 and strong UV radiation. The related SOA tracers were consisted with the emissions of  
257 their precursors including biogenic and anthropogenic VOCs, similar to our previous  
258 studies (Hong et al., 2019; Liu et al., 2020). However, the SOA tracers in winter showed  
259 the lowest concentrations in the morning (8:00–12:00 CST), related with the favorable  
260 dispersion conditions caused by the increasing planetary boundary layer height (BLH)  
261 (Fig.1). Levoglucosan (LEV), a typical tracer of biomass burning, similar seasonal and  
262 diurnal trend to other tracers was observed. However, LEV may not be as stable in the  
263 atmosphere, especially under high relative humidity conditions (Hoffmann et al., 2010).  
264 In this study, maybe, it's hard to reflect the real concentration of LEV. A correlation of  
265 CPA with LEV was carried out (Fig.S2), just to discuss the impacts of biomass burning  
266 on the distribution of CPA tracers through local or long-range transport. Totally, high  
267 concentrations of BSOA tracers was found in the daytime and in summer, indicating  
268 the effects of temperature on biogenic VOCs emissions and their photochemical  
269 oxidations. And the concentrations of BSOA tracers in winter increased in the nighttime,  
270 due to the changing of nocturnal boundary layer.

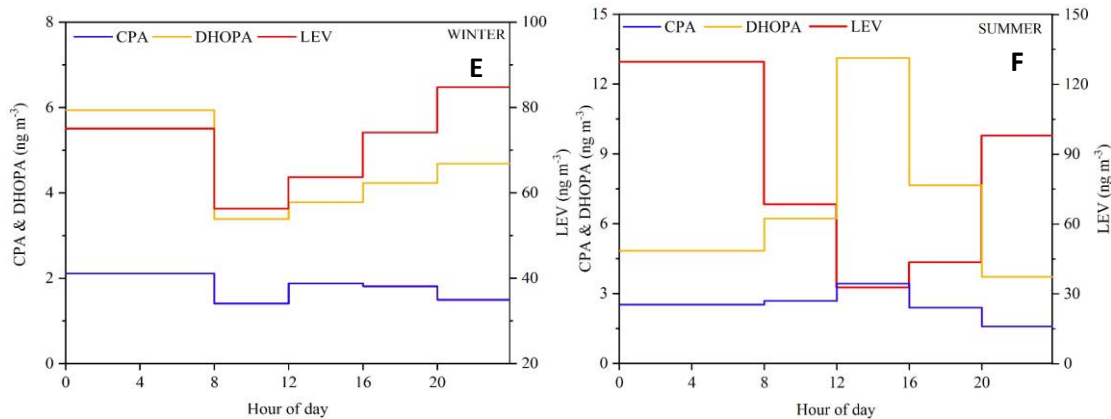
271



272



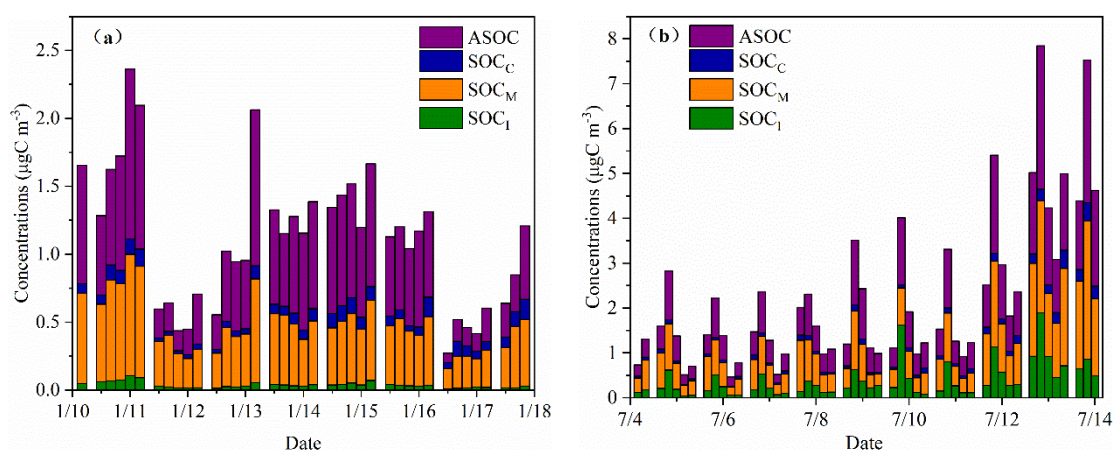
273



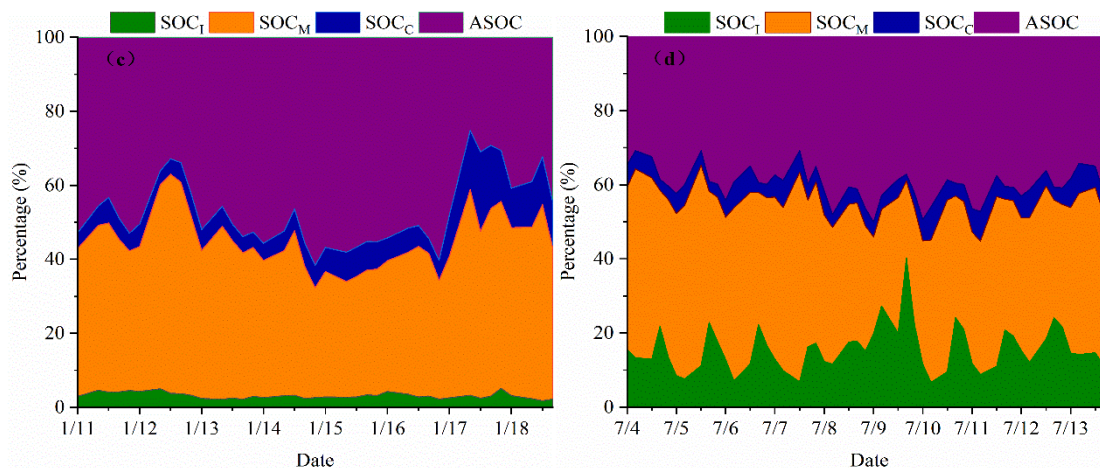
274 **Figure 2. Diurnal variation of individual SOA tracer during the wintertime and**  
 275 **summertime**

276 As shown in Fig.3a, b, SOA tracers-based SOC in winter and summer was  
 277 estimated. The concentrations of SOC in winter ranged from 0.27 to 2.36  $\mu\text{g C m}^{-3}$ , with  
 278 an average of 1.11  $\mu\text{g C m}^{-3}$ . Meanwhile, the concentrations of SOC in summer ranged  
 279 from 0.46 to 7.85  $\mu\text{g C m}^{-3}$ , with an average of 2.27  $\mu\text{g C m}^{-3}$ . The concentrations of  
 280 SOC in summer was higher than that in winter, attributed to the increase of flourishing

281 vegetation emissions and photochemical reactions under high temperature and strong solar  
 282 radiation conditions. For individual SOA tracer, the concentrations of monoterpene-  
 283 derived SOC ( $0.87 \pm 0.64 \mu\text{g C m}^{-3}$ ) was comparable to the toluene-derived SOC ( $0.90$   
 284  $\pm 0.69 \mu\text{g C m}^{-3}$ ), which were higher than isoprene-derived SOC ( $0.39 \pm 0.38 \mu\text{g C m}^{-3}$ )  
 285  $^3$ ) and  $\beta$ -caryophyllene-derived SOC ( $0.10 \pm 0.08 \mu\text{g C m}^{-3}$ ). An obvious trend of  
 286 diurnal variations of isoprene-derived SOC in summer was observed, which was  
 287 consistent with the diurnal pattern of isoprene concentration (Fig.S3). However, no  
 288 similar trend was found in winter, attributed to the influence of low temperature on  
 289 inhibiting the emissions of isoprene from various kinds of plants. In addition, the  
 290 toluene, monoterpene, isoprene and  $\beta$ -caryophyllene-derived SOC in summer  
 291 accounted for 40.0%, 39.2%, 15.7% and 5.1% of the total SOC, respectively (Fig.3c,  
 292 d). However, in winter, the percentages of toluene, monoterpene, isoprene and  $\beta$ -  
 293 caryophyllene-derived SOC were 47.2%, 42.1%, 3.2% and 7.6%, respectively. The  
 294 percentages of isoprene-derived SOC estimated from different precursors varied  
 295 significantly among the seasons. High temperature enhanced the emissions of isoprene,  
 296 and strong solar radiation favored the formation of isoprene SOA tracers, contributing  
 297 to the highest isoprene-derived SOC percentage in summer (Ding et al., 2014). And the  
 298 highest percentages of toluene-derived SOC (47.2%) in winter were related with  
 299 anthropogenic emissions and adverse diffusion conditions.



300

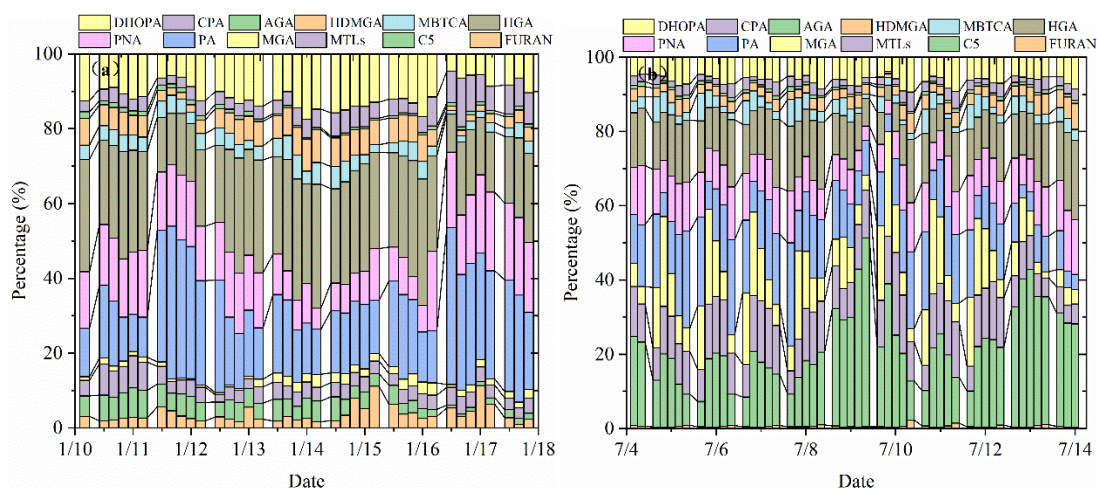


301

302 **Figure 3. Concentrations and percentages of SOA tracer-based estimated SOC**  
 303 **during the sampling period**

304 *3.3 Atmospheric process indication of BSOA tracers*

305 As shown in Fig.4, percentages of different types of SOA tracers in winter and  
 306 summer were calculated. In summer, the monoterpene, isoprene, toluene and  $\beta$ -  
 307 caryophyllene SOA tracers accounted for 45.8%, 45.6%, 6.2% and 2.3% of the total  
 308 SOA tracers, respectively. However, in winter, the percentages of monoterpene,  
 309 isoprene, toluene and  $\beta$ -caryophyllene SOA tracers were 70.1%, 14.0%, 11.0% and  
 310 4.9%, respectively. The percentage of SOA<sub>I</sub> tracers decreased sharply, due to the  
 311 impacts of temperature on isoprene emissions, which was consisted with our previous  
 312 findings (Hong et al., 2019). Meanwhile, the concentrations of SOA<sub>M</sub> tracers were the  
 313 largest in both seasons, due to a large amount of monoterpene emissions from the  
 314 related plant species. Xiamen, an international garden city, located in coastal area of  
 315 southeastern China. Monoterpene, such as  $\alpha/\beta$ -pinene, is mostly emitted by coniferous  
 316 plant and most flowers and fruits, while isoprene originates from broad-leaved trees  
 317 and deciduous plants (Ding et al., 2014; Shrivastava et al., 2017; Yang et al., 2021).



318

319 **Figure 4. Percentages of isoprene, monoterpene,  $\beta$ -caryophyllene and toluene**  
 320 **SOA tracers in winter (a) and summer (b)**

321 The first (PA and PNA) and later generation (HGA, AGA, HDMGA and MBTCA)  
 322 products were used to evaluate the aging degree of SOA<sub>M</sub> (Ding et al., 2014; Hong et  
 323 al., 2019). In this study, HGA (32.2%) was the major component of  $\alpha/\beta$ -pinene tracers,  
 324 followed by PA (30.5%), PNA (21.8%), HDMGA (7.3%), MBTCA (6.8%), and AGA  
 325 (1.5%). The percentage of PA and PNA were much higher than those in mountainous  
 326 background areas (PA: 9% and PNA: 3%)(Hong et al., 2019), suggesting the  
 327 contribution of preliminary products to SOA in urban areas. As shown in Fig.4, the  
 328 percentages of PA and PNA in winter (21.8% and 14.2%) were higher than those in  
 329 summer (14.2% and 10.7%). Reacted with atmospheric oxidants including O<sub>3</sub> and OH,  
 330 PA and PNA were transformed into MBTCA (Offenberg et al., 2007). This is the reason  
 331 why the proportions of PA and PNA had a significant decreasing trend from winter to  
 332 summer. The ratio of MBTCA/(PA+PNA) in summer and winter were  $0.16\pm 0.09$  and  
 333  $0.12\pm 0.07$ , respectively, which also proved the impacts of atmospheric oxidation  
 334 capacity on the aging degree of SOA<sub>M</sub>. In addition, the ratio of HGA/MBTCA could  
 335 be used to distinguish the contribution of  $\alpha$ -pinene or  $\beta$ -pinene to the SOA<sub>M</sub> formation  
 336 (Jaoui et al., 2005; Ding et al., 2014). Low ratio of HGA/MBTCA ( $\sim 1.0$ ) showed that  
 337  $\alpha$ -pinene was the major precursor for SOA<sub>M</sub> (Lewandowski et al., 2013). The ratio of  
 338 HGA/MBTCA with an average of 5.78 in Xiamen was high, suggesting the contribution

339 of  $\beta$ -pinene to SOA<sub>M</sub>.

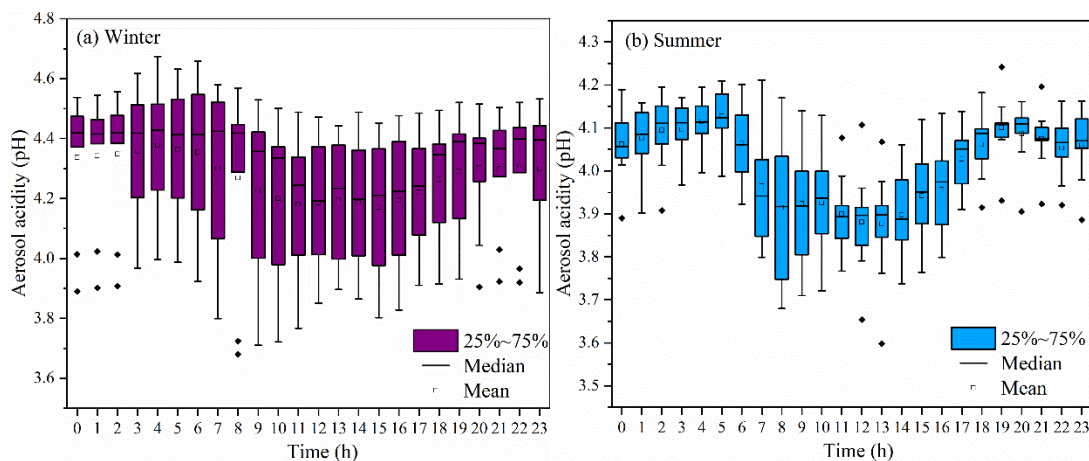
340 As shown in Fig.4, MTLs and C5 alkene triols were the main components of the  
341 total SOA<sub>I</sub>, with an average percentage of  $68.0\pm 14.9\%$ , indicating a low-NOx  
342 environment (Ding et al., 2014; Liu et al., 2020). In summer, the percentages of MTLs  
343 and C5 alkene triols to the total SOA tracers in summer (21.8% and 14.2%) were  
344 obviously higher than those in winter (4.2% and 4.3%). This was consisted with the  
345 fact that the concentrations of NO<sub>2</sub> ( $14.8\pm 7.46 \mu\text{g m}^{-3}$ ) in summer was significantly  
346 lower than that ( $32.7\pm 32.6 \mu\text{g m}^{-3}$ ) in winter. Previous studies found that MTLs and C5  
347 alkene triols were formed by the OH and HO<sub>2</sub> radicals via the HO<sub>2</sub> channel under low-  
348 NOx conditions (Surratt et al., 2010). C5 alkene triols are mainly produced by acid  
349 catalyzed reaction of Isoprene Epoxydiols (IEPOX) in the gas phase, while MTLs are  
350 formed by ring opening products of IEPOX (Surratt et al., 2007; Surratt et al., 2010).  
351 And the ozonolysis of isoprene was also an important pathway for MTLs in the  
352 presence of acid sulfate aerosols (Riva et al., 2016).

353 CPA, the typical tracer of sesquiterpenes, is formed by the photooxidation of  $\beta$ -  
354 caryophyllene (Jaoui et al., 2007). As shown in Fig.4, CPA in winter and summer  
355 accounted for 5.0% and 2.3% of the total SOA tracers, respectively. This is because  
356 that the percentage of SOA<sub>I</sub> has significant increase in summer. And the concentrations  
357 of CPA ( $2.5\pm 2.0 \text{ ng m}^{-3}$ ) in summer were higher than that ( $1.7\pm 0.8 \text{ ng m}^{-3}$ ) in winter,  
358 probably attributed to the emissions of  $\beta$ -caryophyllene driven by temperature and solar  
359 radiation. The CPA has a good correlation with DHOPA in summer (Fig.S2),  
360 suggesting the influence of photochemical oxidation (Liu et al., 2020). However, the  
361 CPA were not correlated with LEV in both seasons, reflecting the limited contribution  
362 of biomass burning (Zhang et al., 2019c).

### 363 *3.4 Impacts of aerosol acidity on BSOA formation*

364 Aerosol acidity (pH) was an important factor on SOA formation (Surratt et al.,  
365 2007; Offenberg et al., 2009; Zhang et al., 2019b; Zhang et al., 2019d). Time series of  
366 aerosol pH calculated by ISORROPIA II is shown in Fig.5. The PM<sub>2.5</sub> in Xiamen was  
367 moderately acidic with daily pH range from 3.68 to 4.67. The highest aerosol pH was

368 observed in winter, and the lowest pH in summer. This is with similar seasonal trend,  
369 closing to the Yangtze River Delta (YRD) region, but obviously lower levels than those  
370 in NCP cities of China (Zhou et al., 2021). In general, the aerosol pH in Chinese cities  
371 were higher than those in US and European.



372

373 **Figure 5. Diurnal variations of aerosol acidity (pH) during the wintertime and**  
374 **summertime period (The boxes with error bars represent the 10th, 25th, 75th,**  
375 **and 90th percentiles)**

376 A declining trend pH during the daytime was observed (Fig. 5), which was related  
377 to the changes of chemical compositions and environmental conditions. The aerosol pH  
378 levels (~3 to 6) was related with a shift from sulfate- to nitrate-dominated aerosols (Guo  
379 et al., 2017). According to the multiphase buffer theory, the peak buffer pH (pKa\*)  
380 regulated the aerosol pH, and temperature could obviously cause the variation of  
381 aerosol pH (Zheng et al., 2020). To further discuss the impacts of aerosol acidity on  
382 BSOA formation in coastal city, we analyzed the relationship between BSOA tracers  
383 and seed particles with different pH and liquid water content (LWC) (Fig. S4 and Table  
384 1).

385 In Table 1, the BSOA tracers was linearly correlated with aerosol acidity (pH) and  
386  $\text{SO}_4^{2-}$ . In summer, BSOA tracers in the particle phase were found to increase with  
387 increasing acidity, which was attributed to the presence of acid catalyzed aerosols. For  
388 example, isoprene SOA tracers is mainly formed through acid-catalyzed reactive  
389 uptake of isoprene-derived epoxydiols (IEPOX) onto sulfate aerosol particles.



390 **Table 1 Correlations between individual BSOA tracer and environmental factors in winter and summer**

Season	SOA tracer	pH	LWC	HONO	PM <sub>2.5</sub>	Cl <sup>-</sup>	NO <sub>3</sub> <sup>-</sup>	SO <sub>4</sub> <sup>2-</sup>	NH <sub>3</sub>	SO <sub>2</sub>	NO <sub>2</sub>	Ox	T	RH	UV
WINTER (n=39)	C5	.584**	.701**	.534**	.690**	.569**	.710**	.663**	.705**	0.308	.353*	0.203	.361*	0.140	0.200
	MTLs	.590**	.705**	.431*	.665**	.639**	.707**	.651**	.757**	0.185	0.229	0.098	.353*	0.295	-0.068
	MGA	.390*	.707**	0.261	.668**	0.081	.758**	.572**	0.284	0.172	0.123	.374*	.377*	-0.019	0.238
	PA	.432*	.403**	.463**	.407**	.481*	.416*	.488*	.440*	.446*	0.241	-0.193	.319*	-0.205	0.145
	PNA	.489**	.579**	0.311	.459**	.516**	.573**	.533**	.543**	0.08	0.071	-0.101	0.121	.337*	-0.122
	HGA	.443*	.829**	.352*	.834**	.600**	.847**	.754**	.641**	0.275	0.299	.451**	.451**	0.043	0.210
	MBTCA	.433*	.678**	.447**	.670**	.435*	.733**	.589**	.710**	.327*	0.253	.492**	.552**	-0.158	0.317
	HDMGA	.421*	.876**	.401*	.867**	.631**	.884**	.813**	.643**	.335*	.321*	.526**	.485**	-0.049	0.327
	AGA	.570**	.575**	.370*	.488**	.577**	.566**	.544**	.731**	0.126	0.181	0.019	0.279	0.298	-0.122
	CPA	0.212	.462**	-0.068	.452**	.483**	.437*	.419*	.255	-0.15	-0.170	0.016	0.079	0.200	-0.144
SUMMER (n=50)	C5	-.495**	.425**	0.160	.622**	-.340*	0.268	.625**	.436**	0.254	0.025	.649**	.573**	-.529**	0.247
	MTLs	-.551**	0.131	0.055	0.272	-.439**	0.131	.428**	.304*	0.089	-0.278	.550**	.610**	-.594**	0.263
	MGA	-.540**	0.029	0.116	0.132	-.403**	0.066	.472**	0.270	0.096	-0.410**	.443**	.633**	-.668**	.382*
	PA	-.633**	.483**	.601**	.461**	-0.135	.541**	.502**	.405*	0.037	0.238	.456**	.626**	-.558**	.400*
	PNA	-.664**	.616**	.387**	.812**	-.389**	.450**	.784**	.503**	0.269	.294*	.769**	.718**	-.631**	.404*
	HGA	-.607**	.612**	.299*	.836**	-.384**	.447**	.770**	.539**	.316*	0.272	.808**	.670**	-.599**	0.322
	MBTCA	-.752**	.415**	0.237	.577**	-.382**	.359*	.636**	.501**	0.201	-0.052	.712**	.852**	-.816**	.588**
	HDMGA	-.525**	.618**	.299*	.833**	-.342*	.408**	.768**	.488**	.358*	.365**	.746**	.574**	-.500**	0.240
	AGA	-.684**	.592**	.447**	.766**	-.334*	.479**	.735**	.435**	0.244	0.271	.694**	.720**	-.634**	.477**
	CPA	-.552**	.625**	.441**	.780**	-.280*	.453**	.763**	.307*	.299*	.503**	.611**	.529**	-.458**	0.305

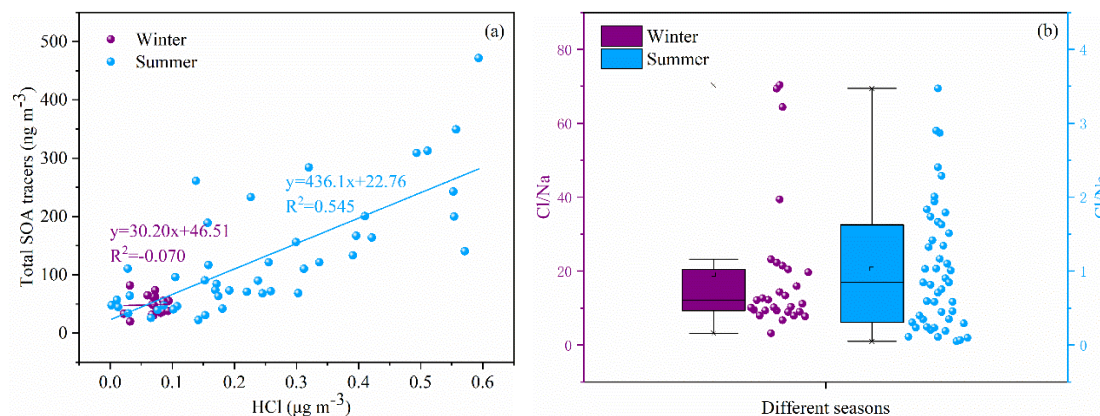
391 \*\*Correlation coefficients with an asterisk indicate statistically significant relationships at  $\alpha = 0.05$ , and two asterisks mean significant at  $\alpha = 0.01$ .

394 In our previous studies, we have reported that high concentration of MTLs was related  
395 with sulfate, which could significantly promote the formation of isoprene-SOA tracers  
396 (Liu et al., 2020). Other studies also found that sulfate could increase the BSOA  
397 production by promoting acid-catalyzed ring-opening reactions (Xu et al., 2015). In  
398 contrast, positive correlations between BSOA tracers and aerosol pH in winter were  
399 observed, indicating that the formation of BSOA was predominantly enhanced by other  
400 factors, except for the aerosol acidity. The aerosol pH in winter was higher than those  
401 in summer, probably due to the influence of nitrate-dominated aerosols. Also, the aged  
402 aerosols through long-range transport might result in the increase of BSOA tracers and  
403 aerosol pH.

404 In addition, positive correlation between BSOA tracers and LWC was observed  
405 (Table 1), probably attributed to the effects of the LWC on determining the peak buffer  
406 pH (pKa\*). Zheng et al. (2020) reported that the buffering effect of ammonia suppresses  
407 the contribution of different chemical compositions in aerosol particles, making LWC  
408 the primary determinant of aerosol pH. Other studies have demonstrated that the uptake  
409 coefficient of first-generation oxidation products, especially for carbonyl compounds,  
410 might depend on RH (Luo et al., 2019). Meanwhile, high LWC could reduce the aerosol  
411 particle viscosity, which was benefit to the generation of the reactive intermediate such  
412 as IEPOX, or other oxidation products of VOC into aqueous-phase of aerosol particles,  
413 thereby promoting the formation of BSOA (Zhang et al., 2019b; Zhang et al., 2019d).

### 414 *3.5 Impacts of chlorine on BSOA formation*

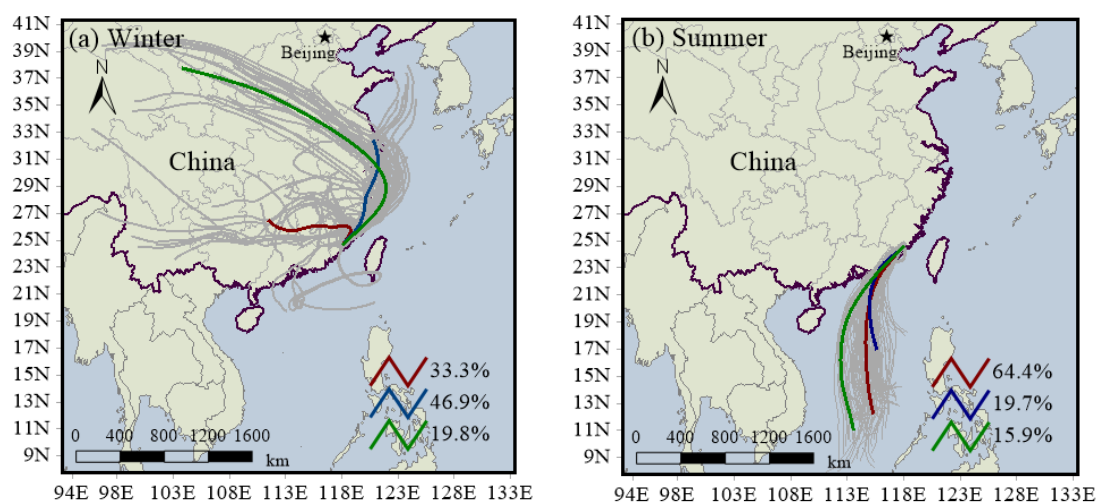
415 Halogen radicals (Cl, Br and I) originated from sea salt aerosol (SSA) have an  
416 important role in tropospheric oxidants chemistry (Wang et al., 2021c). In this study,  
417 chlorine depletion was frequently observed in summer (Fig.6b), indicating that HCl can  
418 be formed through acid displacement of sea salt aerosol  $\text{Cl}^-$  by  $\text{H}_2\text{SO}_4$  and  $\text{HNO}_3$   
419 produced from anthropogenic emissions of  $\text{SO}_2$  and  $\text{NO}_x$ . Moreover, concentrations of  
420 the total SOA tracers were positively correlated with HCl (Fig.6a), suggesting the  
421 enhancement of SOA precursors transformation. Previous studies have found that Cl-  
422 initiated VOC oxidations could contribute to the formation of SOA (Wang and Ruiz,  
423 2017; Dhulipala et al., 2019).



424

425 **Figure 6. Correlations of total SOA tracers and HCl (a) and chlorine depletion**  
 426 **(b) in different seasons**

427 Under ammonia-rich conditions, HCl partitioned into the aqueous particulate  
 428 phase mostly took place, and chlorine ions could affect aqueous oxidation of secondary  
 429 organic compounds (Xu et al., 2021). As shown in Table 1, most of SOA tracers in  
 430 winter were correlated with the concentrations of chlorine ions in PM<sub>2.5</sub>, while inverse  
 431 results were observed in summer. In winter, the dominant wind direction is northeast  
 432 (Fig.7), and chlorine mainly come from continental polluted air mass, such as industrial  
 433 and combustion emissions. So, anthropogenic pollutants through long-range transport  
 434 might cause the enhancement of SOA tracer concentrations at the monitoring site.  
 435 However, in summer, negative correlations of BSOA tracers and chlorine ions in PM<sub>2.5</sub>  
 436 was found, probably due to the influence of chlorine depletion. As shown in Fig. 7, the  
 437 dominant wind direction is southerly, and chlorine mainly originated from the spray of  
 438 sea salt.



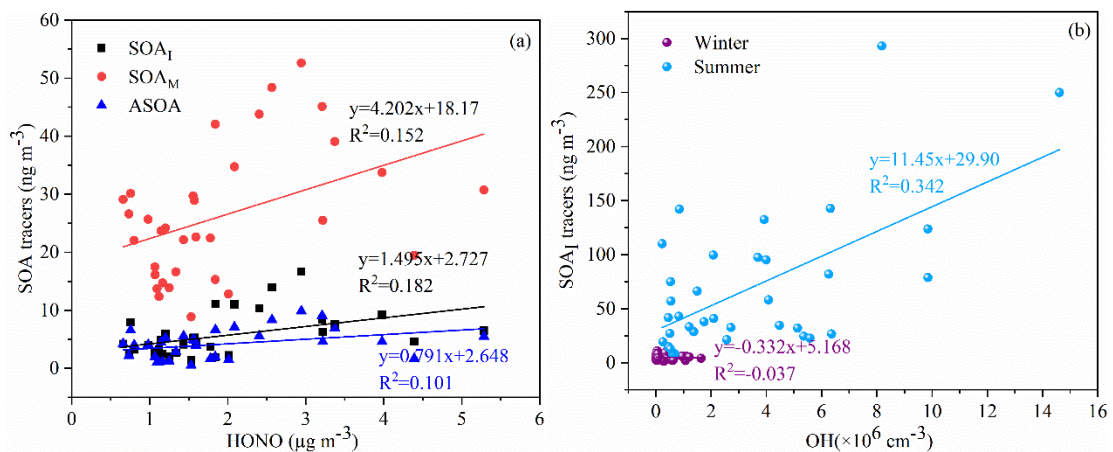
439

440 **Figure 7. Backward trajectories analyses during the winter (a) and summertime**  
 441 **(b)**

442 *3.6. Enhanced formation of BSOA by anthropogenic emissions*

443 Recent studies had indicated that anthropogenic emissions might affect SOA  
 444 formation through multiple chemical processes, based on laboratory studies and field  
 445 observations (Kari et al., 2019; Shrivastava et al., 2019; Zhang et al., 2019c; Cheng et  
 446 al., 2021; Xu et al., 2021). In this study, we conducted the correlation analysis of  
 447 individual SOA tracers and Ox (=O<sub>3</sub>+NO<sub>2</sub>), HONO, OH, SO<sub>2</sub>, NH<sub>3</sub>, PM<sub>2.5</sub>, sulfate,  
 448 nitrate, as well as meteorological parameters (including T, RH and UV) (Table 1).

449 Most of SOA tracers have a significant positive correlation with NH<sub>3</sub>, suggesting  
 450 an enhancement effect on the formation of SOA (Table 1). NH<sub>3</sub> could affect the SOA  
 451 yields through both gas-phase and heterogeneous reactions (Na et al., 2007; Ma et al.,  
 452 2018; Hao et al., 2020). Gas-phase reaction between NH<sub>3</sub> and organic acids (such as  
 453 PA and PNA) produced ammonium salts in the particle phase, which contributed to the  
 454 increased SOA formation. However, not all gas-phase organic acids (e.g., MGA and  
 455 pyruvic acid) could demonstrate gas-to-particle conversion (Na et al., 2007). When  
 456 SOA formation had ceased, the addition of excessive NH<sub>3</sub> would result in the rapid  
 457 decomposition of the main SOA species, due to the nucleophilic attack of NH<sub>3</sub> (Ma et  
 458 al., 2018).



459

460 **Figure 8. Relationships of SOA tracers and HONO and its estimated OH**

461 As an indicator of atmospheric oxidation capacity, the tropospheric odd oxygen  
 462 Ox (O<sub>3</sub>+NO<sub>2</sub>) was calculated. As shown in Table 1, the majority of SOA tracers in  
 463 summer showed significant positive correlations with Ox (R>0.5, P<0.001). However,  
 464 in winter, a part of SOA<sub>M</sub> tracers (e.g. HGA, MBTCA and HDMGA) were found to be

465 significantly correlated with Ox. In addition, HONO and OH radicals, another critical  
466 indicator of atmospheric oxidation capacity, was also discussed. In this study, the  
467 concentration of OH radicals calculated from HONO in summer was higher than those  
468 in winter. In summer, the SOA<sub>I</sub> tracers was correlated with OH radicals (Fig.8b),  
469 consisted with previous findings that OH radicals could promote the formation of SOA  
470 (Sarrafzadeh et al., 2016; Liu et al., 2019; Song et al., 2019; Zhang et al., 2019a). Due  
471 to its photolysis to produce OH radicals during the daytime, HONO could facilitate  
472 SOA formation. In winter, the concentrations of SOA<sub>I</sub>, SOA<sub>M</sub> and ASOA tracers were  
473 correlated with HONO (Fig.8a). These results indicated high concentrations of HONO  
474 and sufficient ultraviolet radiation could enhance the photochemical reactions of VOCs.  
475 Which was consisted with our previous results on the formation of peroxyacetyl nitrate  
476 (PAN) (Hu et al., 2020). As for T and UV, it exhibited significantly positive correlations  
477 with the related SOA tracers, especially in summer. These results suggested that SOA  
478 tracers were produced from the photo-oxidation of VOC precursors (Cheng et al., 2021).

479 In addition, the SOA tracers were significantly positive correlated with PM<sub>2.5</sub> and  
480 its components including NO<sub>3</sub><sup>-</sup> and SO<sub>4</sub><sup>2-</sup>. In coastal cities of southeastern China, with  
481 the development of rapid urbanization, air pollution caused by motor vehicles and  
482 industrial emissions is becoming more frequent in winter (Wu et al., 2020). The Xiamen  
483 port is one of the top 10 ports in China, resulting the impacts of ship emissions and port  
484 activities on ambient air quality (Xu et al., 2018), and the numbers of motor vehicles  
485 increased sharply in recent years. We also found that the 90th percentile of maximum  
486 daily average 8h (MDA8) O<sub>3</sub> concentrations in Xiamen was significantly increased  
487 from 2015 to 2020 (Fig. S5). During the past several years, the elevated secondary  
488 inorganic components, including NO<sub>3</sub><sup>-</sup>, SO<sub>4</sub><sup>2-</sup> and NH<sub>4</sub><sup>+</sup>, accounted for 40-50% of the  
489 total PM<sub>2.5</sub>, and OM ranged from 30% to 40% (Wu et al., 2019; Hong et al., 2021).  
490 These results also implied the effects of anthropogenic emissions and enhanced  
491 atmospheric oxidation capacity on secondary formation of aerosol particles under  
492 atmospheric stagnant conditions.

## 493 **Conclusions**

494 Pollution characteristics and source identification of BSOA tracers during the  
495 summer and winter in coastal areas of southeastern China were investigated. The  
496 average concentration of total BSOA tracers in summer was higher than that in winter,

497 with the predominance of SOA<sub>M</sub>, followed by SOA<sub>I</sub> and SOA<sub>C</sub>. The BSOA tracers in  
498 summer were predominantly produced by the influence of photochemical oxidation  
499 under relatively clean conditions. However, in winter, the formation of BSOA tracers  
500 were attributed to the impacts of anthropogenic emissions and atmospheric stagnant  
501 conditions. In addition, the results also indicated that acid-catalyzed reactive uptake  
502 onto sulfate aerosol particles enhanced the formation of BSOA in both seasons. We  
503 further found that Cl-initiated VOC oxidations has potentially accelerated the  
504 transformation of BSOA precursors through sea salt aerosol originated from the ocean  
505 in summer and anthropogenic emissions in winter. This study demonstrated that the  
506 combined effects of anthropogenic pollutants and atmospheric oxidation capacity on  
507 the formation of BSOA in coastal area.

508

509 **Data Availability.** The data set related to this work can be accessed via  
510 <https://doi.org/10.5281/zenodo.6376025> (Hong, 2022). The details are also available  
511 upon request from the corresponding author (ywhong@iue.ac.cn).

512

513 **Authorship Contribution Statement.** Youwei Hong and Xinbei Xu contributed equally  
514 to this work. Youwei Hong designed and wrote the manuscript. Xinbei Xu collected the  
515 data, contributed to the data analysis. Dan Liao, Taotao Liu, Xiaoting Ji and Ke Xu  
516 performed modeling analyses and data analysis. Jinsheng Chen supported funding of  
517 observation and research. Chunyang Liao, Ting Wang and Chunshui Lin contributed to  
518 revise the manuscript.

519

520 **Competing interests.** The authors declare that they have no conflict of interest.

521

522 **Acknowledgement.** The authors gratefully acknowledge Yanting Chen, Han Zhang and  
523 Xu Liao (Institute of Urban Environment, Chinese Academy of Sciences) for the  
524 guidance and assistance during sample pretreatment, and Lingling Xu and Mengren Li  
525 (Institute of Urban Environment, Chinese Academy of Sciences) for the discussion of  
526 this paper. This study was supported by Fujian Key Laboratory of Atmospheric Ozone  
527 Pollution Prevention and Xiamen Atmospheric Environment Observation and Research  
528 Station of Fujian Province (Institute of Urban Environment, Chinese Academy of  
529 Sciences).

530

531 **Financial support.** This research was financially supported by the Xiamen Youth  
532 Innovation Fund Project (3502Z20206094), the foreign cooperation project of Fujian  
533 Province (2020I0038), the Cultivating Project of Strategic Priority Research Program  
534 of Chinese Academy of Sciences (XDPB1903), the National Key Research and  
535 Development Program (2016YFC0112200), State Key Laboratory of Environmental  
536 Chemistry and Ecotoxicology, Research Center for Eco-Environmental Sciences, CAS  
537 (KF2020-06), the FJIRSM&IUE Joint Research Fund (RHZX-2019-006) and center for  
538 Excellence in Regional Atmospheric Environment project (E0L1B20201).

539

## 540 Reference

- 541 Charan, S. M., Huang, Y., and Seinfeld, J. H.: Computational Simulation of Secondary  
542 Organic Aerosol Formation in Laboratory Chambers, *Chem. Rev.*, 119, 11912-11944,  
543 10.1021/acs.chemrev.9b00358, 2019.
- 544 Cheng, Y., Ma, Y., and Hu, D.: Tracer-based source apportioning of atmospheric organic  
545 carbon and the influence of anthropogenic emissions on secondary organic aerosol  
546 formation in Hong Kong, *Atmos. Chem. Phys.*, 21, 10589-10608, 10.5194/acp-21-  
547 10589-2021, 2021.
- 548 Dhulipala, S. V., Bhandari, S., and Hildebrandt Ruiz, L.: Formation of oxidized organic  
549 compounds from Cl-initiated oxidation of toluene, *Atmospheric Environment*, 199, 265-  
550 273, 10.1016/j.atmosenv.2018.11.002, 2019.
- 551 Ding, X., He, Q.-F., Shen, R.-Q., Yu, Q.-Q., and Wang, X.-M.: Spatial distributions of  
552 secondary organic aerosols from isoprene, monoterpenes, beta-caryophyllene, and  
553 aromatics over China during summer, *Journal of Geophysical Research-Atmospheres*,  
554 119, 11877-11891, 10.1002/2014jd021748, 2014.
- 555 Fountoukis, C., and Nenes, A.: ISORROPIA II: a computationally efficient  
556 thermodynamic equilibrium model for  $K^+Ca^{2+}Mg^{2+}NH_4^+Na^+SO_4^{2-}$  –  
557  $NO_3^-Cl^-H_2O$  aerosols, *Atmos. Chem. Phys.*, 7, 4639-4659, 10.5194/acp-7-  
558 4639-2007, 2007.
- 559 Fu, P., Kawamura, K., Chen, J., and Barrie, L. A.: Isoprene, Monoterpene, and Sesquiterpene  
560 Oxidation Products in the High Arctic Aerosols during Late Winter to Early Summer,  
561 *Environmental Science & Technology*, 43, 4022-4028, 10.1021/es803669a, 2009.
- 562 Guo, H., Sullivan, A. P., Campuzano-Jost, P., Schroder, J. C., Lopez-Hilfiker, F. D.,  
563 Dibb, J. E., Jimenez, J. L., Thornton, J. A., Brown, S. S., Nenes, A., and Weber,  
564 R. J.: Fine particle pH and the partitioning of nitric acid during winter in the  
565 northeastern United States, *Journal of Geophysical Research: Atmospheres*, 121,  
566 10,355-310,376, <https://doi.org/10.1002/2016JD025311>, 2016.
- 567 Guo, H., Weber, R. J., and Nenes, A.: High levels of ammonia do not raise fine particle pH  
568 sufficiently to yield nitrogen oxide-dominated sulfate production, *Scientific Reports*, 7,  
569 12109, 10.1038/s41598-017-11704-0, 2017.
- 570 Hallquist, M., Wenger, J. C., Baltensperger, U., Rudich, Y., Simpson, D., Claeys, M.,  
571 Dommen, J., Donahue, N. M., George, C., Goldstein, A. H., Hamilton, J. F., Herrmann,  
572 H., Hoffmann, T., Iinuma, Y., Jang, M., Jenkin, M. E., Jimenez, J. L., Kiendler-Scharr,  
573 A., Maenhaut, W., McFiggans, G., Mentel, T. F., Monod, A., Prevot, A. S. H., Seinfeld,  
574 J. H., Surratt, J. D., Szmigielski, R., and Wildt, J.: The formation, properties and impact

575 of secondary organic aerosol: current and emerging issues, *Atmospheric Chemistry and*  
576 *Physics*, 9, 5155-5236, 10.5194/acp-9-5155-2009, 2009.

577 Hao, L., Kari, E., Leskinen, A., Worsnop, D. R., and Virtanen, A.: Direct contribution of  
578 ammonia to  $\alpha$ -pinene secondary organic aerosol formation, *Atmos. Chem. Phys.*, 20,  
579 14393-14405, 10.5194/acp-20-14393-2020, 2020.

580 Hoffmann, D., Tilgner, A., Iinuma, Y., and Herrmann, H.: Atmospheric Stability of  
581 Levoglucosan: A Detailed Laboratory and Modeling Study, *Environmental Science &*  
582 *Technology*, 44, 694-699, 10.1021/es902476f, 2010.

583 Hong, Y., Xu, X., Liao, D., Zheng, R., Ji, X., Chen, Y., Xu, L., Li, M., Wang, H., Xiao, H.,  
584 Choi, S.-D., and Chen, J.: Source apportionment of PM<sub>2.5</sub> and sulfate formation during  
585 the COVID-19 lockdown in a coastal city of southeast China, *Environmental Pollution*,  
586 286, 117577, <https://doi.org/10.1016/j.envpol.2021.117577>, 2021.

587 Hong, youwei. (2022). Dataset for ACP by Hong et al., 2022 [Data set]. Zenodo.  
588 <https://doi.org/10.5281/zenodo.6376025>

589 Hong, Z., Zhang, H., Zhang, Y., Xu, L., Liu, T., Xiao, H., Hong, Y., Chen, J., Li, M., Deng,  
590 J., Wu, X., Hu, B., and Chen, X.: Secondary organic aerosol of PM<sub>2.5</sub> in a mountainous  
591 forest area in southeastern China: Molecular compositions and tracers implication,  
592 *Science of the Total Environment*, 653, 496-503, 10.1016/j.scitotenv.2018.10.370, 2019.

593 Hoyle, C. R., Boy, M., Donahue, N. M., Fry, J. L., Glasius, M., Guenther, A., Hallar, A. G.,  
594 Hartz, K. H., Petters, M. D., Petaja, T., Rosenoern, T., and Sullivan, A. P.: A review of  
595 the anthropogenic influence on biogenic secondary organic aerosol, *Atmospheric*  
596 *Chemistry and Physics*, 11, 321-343, 10.5194/acp-11-321-2011, 2011.

597 Hu, B., Liu, T., Hong, Y., Xu, L., Li, M., Wu, X., Wang, H., Chen, J., and Chen, J.:  
598 Characteristics of peroxyacetyl nitrate (PAN) in a coastal city of southeastern China:  
599 Photochemical mechanism and pollution process, *Science of the Total Environment*,  
600 719, 10.1016/j.scitotenv.2020.137493, 2020.

601 Jaoui, M., Kleindienst, T. E., Lewandowski, M., Offenberg, J. H., and Edney, E. O.:  
602 Identification and quantification of aerosol polar oxygenated compounds bearing  
603 carboxylic or hydroxyl groups. 2. Organic tracer compounds from monoterpenes,  
604 *Environmental Science & Technology*, 39, 5661-5673, 10.1021/es048111b, 2005.

605 Jaoui, M., Lewandowski, M., Kleindienst, T. E., Offenberg, J. H., and Edney, E. O.:  $\beta$ -  
606 caryophyllinic acid: An atmospheric tracer for  $\beta$ -caryophyllene secondary organic  
607 aerosol, *Geophysical Research Letters*, 34, 10.1029/2006gl028827, 2007.

608 Kari, E., Hao, L. Q., Ylisirnio, A., Buchholz, A., Leskinen, A., Yli-Pirila, P., Nuutinen, I.,  
609 Kuuspallo, K., Jokiniemi, J., Faiola, C. L., Schobesberger, S., and Virtanen, A.: Potential  
610 dual effect of anthropogenic emissions on the formation of biogenic secondary organic  
611 aerosol (BSOA), *Atmospheric Chemistry and Physics*, 19, 15651-15671, 10.5194/acp-  
612 19-15651-2019, 2019.

613 Kleindienst, T. E., Jaoui, M., Lewandowski, M., Offenberg, J. H., Lewis, C. W., Bhawe, P. V.,  
614 and Edney, E. O.: Estimates of the contributions of biogenic and anthropogenic  
615 hydrocarbons to secondary organic aerosol at a southeastern US location, *Atmospheric*  
616 *Environment*, 41, 8288-8300, 10.1016/j.atmosenv.2007.06.045, 2007.

617 Lewandowski, M., Piletic, I. R., Kleindienst, T. E., Offenberg, J. H., Beaver, M. R., Jaoui, M.,  
618 Docherty, K. S., and Edney, E. O.: Secondary organic aerosol characterisation at field  
619 sites across the United States during the spring-summer period, *International Journal of*  
620 *Environmental Analytical Chemistry*, 93, 1084-1103, 10.1080/03067319.2013.803545,  
621 2013.

622 Liu, S., Tsona, N. T., Zhang, Q., Jia, L., Xu, Y., and Du, L.: Influence of relative humidity on  
623 cyclohexene SOA formation from OH photooxidation, *Chemosphere*, 231, 478-486,  
624 10.1016/j.chemosphere.2019.05.131, 2019.

625 Liu, S., Huang, D., Wang, Y., Zhang, S., Wu, C., Du, W., and Wang, G.: Synergetic effect of  
626 NH<sub>3</sub> and NO<sub>x</sub> on the production and optical absorption of secondary organic aerosol



627 formation from toluene photooxidation, *Atmos. Chem. Phys. Discuss.*, 2021, 1-38,  
628 10.5194/acp-2021-560, 2021.

629 Liu, T., Hu, B., Xu, X., Hong, Y., Zhang, Y., Wu, X., Xu, L., Li, M., Chen, Y., Chen, X., and  
630 Chen, J.: Characteristics of PM<sub>2.5</sub>-bound secondary organic aerosol tracers in a coastal  
631 city in Southeastern China: Seasonal patterns and pollution identification, *Atmospheric  
632 Environment*, 237, 10.1016/j.atmosenv.2020.117710, 2020.

633 Lowes, S., Jersey, J., Shoup, R., Garofolo, F., Savoie, N., Mortz, E., Needham, S., Caturla, M.  
634 C., Steffen, R., Sheldon, C., Hayes, R., Samuels, T., Di Donato, L., Kamerud, J.,  
635 Michael, S., Lin, Z. P., Hillier, J., Moussallie, M., Teixeira, L. D., Rocci, M., Buonarati,  
636 M., Truog, J., Hussain, S., Lundberg, R., Breau, A., Zhang, T. Y., Jonker, J., Berger, N.,  
637 Gagnon-Carignan, S., Nehls, C., Nicholson, R., Hilhorst, M., Karnik, S., de Boer, T.,  
638 Houghton, R., Smith, K., Cojocar, L., Allen, M., Harter, T., Fatmi, S., Sayyarpour, F.,  
639 Vija, J., Malone, M., and Heller, D.: Recommendations on: internal standard criteria,  
640 stability, incurred sample reanalysis and recent 483s by the Global CRO Council for  
641 Bioanalysis, *Bioanalysis*, 3, 1323-1332, 10.4155/Bio.11.135, 2011.

642 Luo, H., Jia, L., Wan, Q., An, T., and Wang, Y.: Role of liquid water in the formation of O-3  
643 and SOA particles from 1,2,3-trimethylbenzene, *Atmospheric Environment*, 217,  
644 10.1016/j.atmosenv.2019.116955, 2019.

645 Lv, S., Wang, F., Wu, C., Chen, Y., Liu, S., Zhang, S., Li, D., Du, W., Zhang, F., Wang, H.,  
646 Huang, C., Fu, Q., Duan, Y., and Wang, G.: Gas-to-Aerosol Phase Partitioning of  
647 Atmospheric Water-Soluble Organic Compounds at a Rural Site in China: An Enhancing  
648 Effect of NH<sub>3</sub> on SOA Formation, *Environmental Science & Technology*,  
649 10.1021/acs.est.1c06855, 2022.

650 Ma, Q., Lin, X. X., Yang, C. G., Long, B., Gai, Y. B., and Zhang, W. J.: The influences of  
651 ammonia on aerosol formation in the ozonolysis of styrene: roles of Criegee intermediate  
652 reactions, *Roy Soc Open Sci*, 5, ARTN 17217110.1098/rsos.172171, 2018.

653 Mahilang, M., Deb, M. K., and Pervez, S.: Biogenic secondary organic aerosols: A review on  
654 formation mechanism, analytical challenges and environmental impacts, *Chemosphere*,  
655 262, 10.1016/j.chemosphere.2020.127771, 2021.

656 McFiggans, G., Mentel, T. F., Wildt, J., Pullinen, I., Kang, S., Kleist, E., Schmitt, S.,  
657 Springer, M., Tillmann, R., Wu, C., Zhao, D. F., Hallquist, M., Faxon, C., Le Breton, M.,  
658 Hallquist, A. M., Simpson, D., Bergstrom, R., Jenkin, M. E., Ehn, M., Thornton, J. A.,  
659 Alfarra, M. R., Bannan, T. J., Percival, C. J., Priestley, M., Topping, D., and Kiendler-  
660 Scharr, A.: Secondary organic aerosol reduced by mixture of atmospheric vapours,  
661 *Nature*, 565, 587-593, 10.1038/s41586-018-0871-y, 2019.

662 Na, K., Song, C., Switzer, C., and Cocker, D. R.: Effect of Ammonia on Secondary Organic  
663 Aerosol Formation from  $\alpha$ -Pinene Ozonolysis in Dry and Humid Conditions,  
664 *Environmental Science & Technology*, 41, 6096-6102, 10.1021/es061956y, 2007.

665 Newland, M. J., Bryant, D. J., Dunmore, R. E., Bannan, T. J., Acton, W. J. F., Langford, B.,  
666 Hopkins, J. R., Squires, F. A., Dixon, W., Drysdale, W. S., Ivatt, P. D., Evans, M. J.,  
667 Edwards, P. M., Whalley, L. K., Heard, D. E., Slater, E. J., Woodward-Massey, R., Ye,  
668 C., Mehra, A., Worrall, S. D., Bacak, A., Coe, H., Percival, C. J., Hewitt, C. N., Lee, J.  
669 D., Cui, T., Surratt, J. D., Wang, X., Lewis, A. C., Rickard, A. R., and Hamilton, J. F.:  
670 Low-NO atmospheric oxidation pathways in a polluted megacity, *Atmos. Chem. Phys.*,  
671 21, 1613-1625, 10.5194/acp-21-1613-2021, 2021.

672 Offenberg, J. H., Lewis, C. W., Lewandowski, M., Jaoui, M., Kleindienst, T. E., and Edney,  
673 E. O.: Contributions of toluene and alpha-pinene to SOA formed in an irradiated  
674 toluene/alpha-pinene/NO<sub>x</sub>/air mixture: Comparison of results using C-14 content and  
675 SOA organic tracer methods, *Environmental Science & Technology*, 41, 3972-3976,  
676 10.1021/es070089+, 2007.

677 Offenberg, J. H., Lewandowski, M., Edney, E. O., Kleindienst, T. E., and Jaoui, M.: Influence  
678 of Aerosol Acidity on the Formation of Secondary Organic Aerosol from Biogenic

679 Precursor Hydrocarbons, *Environmental Science & Technology*, 43, 7742-7747,  
680 10.1021/es901538e, 2009.

681 Palmer, P. I., Marvin, M. R., Siddans, R., Kerridge, B. J., and Moore, D. P.: Nocturnal  
682 survival of isoprene linked to formation of upper tropospheric organic aerosol, *Science*,  
683 375, 562-566, doi:10.1126/science.abg4506, 2022.

684 Reid, J. P., Bertram, A. K., Topping, D. O., Laskin, A., Martin, S. T., Petters, M. D., Pope, F.  
685 D., and Rovelli, G.: The viscosity of atmospherically relevant organic particles, *Nature*  
686 *Communications*, 9, 10.1038/s41467-018-03027-z, 2018.

687 Riva, M., Budisulistiorini, S. H., Zhang, Z., Gold, A., and Surratt, J. D.: Chemical  
688 characterization of secondary organic aerosol constituents from isoprene ozonolysis in  
689 the presence of acidic aerosol, *Atmospheric Environment*, 130, 5-13,  
690 10.1016/j.atmosenv.2015.06.027, 2016.

691 Rumsey, I. C., Cowen, K. A., Walker, J. T., Kelly, T. J., Hanft, E. A., Mishoe, K.,  
692 Rogers, C., Proost, R., Beachley, G. M., Lear, G., Frelink, T., and Otjes, R. P.:  
693 An assessment of the performance of the Monitor for AeRosols and GAses in  
694 ambient air (MARGA): a semi-continuous method for soluble compounds,  
695 *Atmos. Chem. Phys.*, 14, 5639-5658, 10.5194/acp-14-5639-2014, 2014.

696 Sarrafzadeh, M., Wildt, J., Pullinen, I., Springer, M., Kleist, E., Tillmann, R., Schmitt, S. H.,  
697 Wu, C., Mentel, T. F., Zhao, D., Hastie, D. R., and Kiendler-Scharr, A.: Impact of NO<sub>x</sub>  
698 and OH on secondary organic aerosol formation from beta-pinene photooxidation,  
699 *Atmospheric Chemistry and Physics*, 16, 11237-11248, 10.5194/acp-16-11237-2016,  
700 2016.

701 Shrivastava, M., Cappa, C. D., Fan, J., Goldstein, A. H., Guenther, A. B., Jimenez, J. L.,  
702 Kuang, C., Laskin, A., Martin, S. T., Ng, N. L., Petaja, T., Pierce, J. R., Rasch, P. J.,  
703 Roldin, P., Seinfeld, J. H., Shilling, J., Smith, J. N., Thornton, J. A., Volkamer, R.,  
704 Wang, J., Worsnop, D. R., Zaveri, R. A., Zelenyuk, A., and Zhang, Q.: Recent advances  
705 in understanding secondary organic aerosol: Implications for global climate forcing,  
706 *Reviews of Geophysics*, 55, 509-559, 10.1002/2016rg000540, 2017.

707 Shrivastava, M., Andreae, M. O., Artaxo, P., Barbosa, H. M. J., Berg, L. K., Brito, J., Ching,  
708 J., Easter, R. C., Fan, J., Fast, J. D., Feng, Z., Fuentes, J. D., Glasius, M., Goldstein, A.  
709 H., Alves, E. G., Gomes, H., Gu, D., Guenther, A., Jathar, S. H., Kim, S., Liu, Y., Lou,  
710 S., Martin, S. T., McNeill, V. F., Medeiros, A., de Sa, S. S., Shilling, J. E., Springston, S.  
711 R., Souza, R. A. F., Thornton, J. A., Isaacman-VanWertz, G., Yee, L. D., Ynoue, R.,  
712 Zaveri, R. A., Zelenyuk, A., and Zhao, C.: Urban pollution greatly enhances formation of  
713 natural aerosols over the Amazon rainforest, *Nature Communications*, 10,  
714 10.1038/s41467-019-08909-4, 2019.

715 Song, M., Zhang, C., Wu, H., Mu, Y., Ma, Z., Zhang, Y., Liu, J., and Li, X.: The influence of  
716 OH concentration on SOA formation from isoprene photooxidation, *Science of the Total*  
717 *Environment*, 650, 951-957, 10.1016/j.scitotenv.2018.09.084, 2019.

718 Surratt, J. D., Lewandowski, M., Offenberg, J. H., Jaoui, M., Kleindienst, T. E., Edney, E. O.,  
719 and Seinfeld, J. H.: Effect of acidity on secondary organic aerosol formation from  
720 isoprene, *Environmental Science & Technology*, 41, 5363-5369, 10.1021/es0704176,  
721 2007.

722 Surratt, J. D., Chan, A. W. H., Eddingsaas, N. C., Chan, M., Loza, C. L., Kwan, A. J., Hersey,  
723 S. P., Flagan, R. C., Wennberg, P. O., and Seinfeld, J. H.: Reactive intermediates  
724 revealed in secondary organic aerosol formation from isoprene, *Proceedings of the*  
725 *National Academy of Sciences of the United States of America*, 107, 6640-6645,  
726 10.1073/pnas.0911114107, 2010.

727 Wang, D. S., and Ruiz, L. H.: Secondary organic aerosol from chlorine-initiated oxidation of  
728 isoprene, *Atmos. Chem. Phys.*, 17, 13491-13508, 10.5194/acp-17-13491-2017, 2017.

729 Wang, J., Ye, J., Zhang, Q., Zhao, J., Wu, Y., Li, J., Liu, D., Li, W., Zhang, Y., Wu, C., Xie,  
730 C., Qin, Y., Lei, Y., Huang, X., Guo, J., Liu, P., Fu, P., Li, Y., Lee, H. C., Choi, H.,  
731 Zhang, J., Liao, H., Chen, M., Sun, Y., Ge, X., Martin, S. T., and Jacob, D. J.: Aqueous

732 production of secondary organic aerosol from fossil-fuel emissions in winter Beijing  
733 haze, *Proc Natl Acad Sci U S A*, 118, 10.1073/pnas.2022179118, 2021a.

734 Wang, J., Ye, J., Zhang, Q., Zhao, J., Wu, Y., Li, J., Liu, D., Li, W., Zhang, Y., Wu, C., Xie,  
735 C., Qin, Y., Lei, Y., Huang, X., Guo, J., Liu, P., Fu, P., Li, Y., Lee, H. C., Choi, H.,  
736 Zhang, J., Liao, H., Chen, M., Sun, Y., Ge, X., Martin, S. T., and Jacob, D. J.: Aqueous  
737 production of secondary organic aerosol from fossil-fuel emissions in winter Beijing  
738 haze, *Proceedings of the National Academy of Sciences of the United States of America*,  
739 118, 10.1073/pnas.2022179118, 2021b.

740 Wang, S., Du, L., Tsona, N. T., Jiang, X., You, B., Xu, L., Yang, Z., and Wang, W.: Effect of  
741 NO<sub>x</sub> and SO<sub>2</sub> on the photooxidation of methylglyoxal: Implications in secondary  
742 aerosol formation, *J Environ Sci (China)*, 92, 151-162, 10.1016/j.jes.2020.02.011, 2020.

743 Wang, X., Jacob, D. J., Downs, W., Zhai, S., Zhu, L., Shah, V., Holmes, C. D., Sherwen, T.,  
744 Alexander, B., Evans, M. J., Eastham, S. D., Neuman, J. A., Veres, P. R., Koenig, T. K.,  
745 Volkamer, R., Huey, L. G., Bannan, T. J., Percival, C. J., Lee, B. H., and Thornton, J. A.:  
746 Global tropospheric halogen (Cl, Br, I) chemistry and its impact on oxidants, *Atmos.*  
747 *Chem. Phys.*, 21, 13973-13996, 10.5194/acp-21-13973-2021, 2021c.

748 Wen, L., Chen, T., Zheng, P., Wu, L., Wang, X., Mellouki, A., Xue, L., and Wang, W.:  
749 Nitrous acid in marine boundary layer over eastern Bohai Sea, China: Characteristics,  
750 sources, and implications, *Sci. Total Environ.*, 10.1016/j.scitotenv.2019.03.225, 2019.

751 Wu, X., Xu, L. L., Hong, Y. W., Chen, J. F., Qiu, Y. Q., Hu, B. Y., Hong, Z. Y., Zhang, Y.  
752 R., Liu, T. T., Chen, Y. T., Bian, Y. H., Zhao, G. Q., Chen, J. S., and Li, M. R.: The air  
753 pollution governed by subtropical high in a coastal city in Southeast China: Formation  
754 processes and influencing mechanisms, *Science of the Total Environment*, 692, 1135-  
755 1145, 10.1016/j.scitotenv.2019.07.341, 2019.

756 Wu, X., Li, M., Chen, J., Wang, H., Xu, L., Hong, Y., Zhao, G., Hu, B., Zhang, Y., Dan, Y.,  
757 and Yu, S.: The characteristics of air pollution induced by the quasi-stationary front:  
758 Formation processes and influencing factors, *Science of the Total Environment*, 707,  
759 10.1016/j.scitotenv.2019.136194, 2020.

760 Xiao, Y., Wu, Z., Guo, S., He, L., Huang, X., and Hu, M.: Formation mechanism of  
761 secondary organic aerosol in aerosol liquid water: A review, *Chinese Science Bulletin*,  
762 65, 3118-3133, 2020.

763 Xu, L., Du, L., Tsona, N. T., and Ge, M. F.: Anthropogenic Effects on Biogenic Secondary  
764 Organic Aerosol Formation, *Advances in Atmospheric Sciences*, 38, 1053-1084,  
765 10.1007/s00376-020-0284-3, 2021.

766 Xu, L., Guo, H. Y., Boyd, C. M., Klein, M., Bougiatioti, A., Cerully, K. M., Hite, J. R.,  
767 Isaacman-VanWertz, G., Kreisberg, N. M., Knote, C., Olson, K., Koss, A., Goldstein, A.  
768 H., Hering, S. V., de Gouw, J., Baumann, K., Lee, S. H., Nenes, A., Weber, R. J., and  
769 Ng, N. L.: Effects of anthropogenic emissions on aerosol formation from isoprene and  
770 monoterpenes in the southeastern United States, *Proceedings of the National Academy of*  
771 *Sciences of the United States of America*, 112, 37-42, 10.1073/pnas.1417609112, 2015.

772 Yang, W., Cao, J., Wu, Y., Kong, F., and Li, L.: Review on plant terpenoid emissions  
773 worldwide and in China, *The Science of the total environment*, 787, 147454-147454,  
774 10.1016/j.scitotenv.2021.147454, 2021.

775 Zhang, J., An, J., Qu, Y., Liu, X., and Chen, Y.: Impacts of potential HONO sources on the  
776 concentrations of oxidants and secondary organic aerosols in the Beijing-Tianjin-Hebei  
777 region of China, *Science of the Total Environment*, 647, 836-852,  
778 10.1016/j.scitotenv.2018.08.030, 2019a.

779 Zhang, P., Chen, T., Liu, J., Liu, C., Ma, J., Ma, Q., Chu, B., and He, H.: Impacts of SO<sub>2</sub>,  
780 Relative Humidity, and Seed Acidity on Secondary Organic Aerosol Formation in the  
781 Ozonolysis of Butyl Vinyl Ether, *Environmental Science & Technology*, 53, 8845-8853,  
782 10.1021/acs.est.9b02702, 2019b.

783 Zhang, Y.-Q., Chen, D.-H., Ding, X., Li, J., Zhang, T., Wang, J.-Q., Cheng, Q., Jiang, H.,  
784 Song, W., Ou, Y.-B., Ye, P.-L., Zhang, G., and Wang, X.-M.: Impact of anthropogenic

785 emissions on biogenic secondary organic aerosol: observation in the Pearl River Delta,  
786 southern China, *Atmospheric Chemistry and Physics*, 19, 14403-14415, 10.5194/acp-19-  
787 14403-2019, 2019c.

788 Zhang, Y., Chen, Y., Lei, Z., Olson, N. E., Riva, M., Koss, A. R., Zhang, Z., Gold, A., Jayne,  
789 J. T., Worsnop, D. R., Onasch, T. B., Kroll, J. H., Turpin, B. J., Ault, A. P., and Surratt,  
790 J. D.: Joint Impacts of Acidity and Viscosity on the Formation of Secondary Organic  
791 Aerosol from Isoprene Epoxydiols (IEPD<sub>X</sub>) in Phase Separated Particles, *ACS Earth and*  
792 *Space Chemistry*, 3, 2646-2658, 10.1021/acsearthspacechem.9b00209, 2019d.

793 Zhao, D. F., Schmitt, S. H., Wang, M. J., Acir, I. H., Tillmann, R., Tan, Z. F., Novelli, A.,  
794 Fuchs, H., Pullinen, I., Wegener, R., Rohrer, F., Wildt, J., Kiendler-Scharr, A., Wahner,  
795 A., and Mentel, T. F.: Effects of NO<sub>x</sub> and SO<sub>2</sub> on the secondary organic aerosol  
796 formation from photooxidation of alpha-pinene and limonene, *Atmospheric Chemistry*  
797 *and Physics*, 18, 1611-1628, 10.5194/acp-18-1611-2018, 2018.

798 Zheng, G., Su, H., Wang, S., Andreae, M. O., Poschl, U., and Cheng, Y.: Multiphase buffer  
799 theory explains contrasts in atmospheric aerosol acidity, *Science*, 369, 1374-+,  
800 10.1126/science.aba3719, 2020.

801 Zhou, M., Zheng, G., Wang, H., Qiao, L., Zhu, S., Huang, D., An, J., Lou, S., Tao, S., Wang,  
802 Q., Yan, R., Ma, Y., Chen, C., Cheng, Y., Su, H., and Huang, C.: Long-term trends and  
803 drivers of aerosol pH in eastern China, *Atmos. Chem. Phys. Discuss.*, 2021, 1-21,  
804 10.5194/acp-2021-455, 2021.

805 Zhu, J., Penner, J. E., Yu, F., Sillman, S., Andreae, M. O., and Coe, H.: Decrease in radiative  
806 forcing by organic aerosol nucleation, climate, and land use change, *Nature*  
807 *Communications*, 10, 10.1038/s41467-019-08407-7, 2019.

808

809

810